Typhoon-induced, highly nonlinear internal solitary waves off the east coast of Korea

SungHyun Nam,[1,2] Duk-jin Kim,[3] Hyoung Rok Kim,[4] and Young-Gyu Kim[4]

Received 14 September 2006; revised 21 November 2006; accepted 8 December 2006; published 11 January 2007.

[1] Highly nonlinear internal solitary waves (ISWs) propagating both onshore and offshore were detected in a SAR image taken approximately 19 hours after typhoon MAEMI's passage across the east coast of Korea. Analysis of ocean buoy data suggests that the ISWs were generated by near-inertial waves in response to typhoon wind. The near-inertial waves can propagate seaward due to a downwelling coastal jet (positive relative vorticity offshore of the jet), and interact with sharply varying topography, producing the ISWs. The area of sharply varying topography approximately 28 km off the coast is suggested as a source region for the ISWs. Simple calculations of wave speed based on the two-layered Korteweg-deVries (KdV) equation with upper layer thickness and densities at both layers fixed indicate that the ISWs were generated 6 hours prior to the time of the acquisition of the SAR image (approximately 13 hours after the typhoon passage), consistent with simultaneous buoy measurements. **Citation:** Nam, S., D. Kim, H. R. Kim, and Y.-G. Kim (2007), Typhoon-induced, highly nonlinear internal solitary waves off the east coast of Korea, *Geophys. Res. Lett.*, *34*, L01607, doi:10.1029/2006GL028187.

1. Introduction

[2] Through the surface manifestation of synthetic aperture radar (SAR) images, highly nonlinear internal solitary waves (ISWs) have been frequently observed in world oceans [*Alpers*, 1985], i.e. continental shelves [*Moum et al.*, 2003], marginal seas [*Klymak et al.*, 2006], straits [*Brandt et al.*, 1997], etc. Spatial characteristics of the highly nonlinear ISWs are diverse depending on locations and time, implying that the generation as well as the evolution of the waves is not a single process. Recently, it has been accepted that the interaction between internal tides and topographic features generate highly nonlinear ISWs [*Zhao et al.*, 2004; *Moum et al.*, 2003]. Large-amplitude ISWs can also be generated associated with a river plume [*Nash and Moum*, 2005]. Moreover, the near-inertial internal waves as well as internal tides provide energy for highly nonlinear ISWs [*Kim et al.*, 2001].

[3] In the coastal region off the east coast of Korea (Figure 1), both semidiurnal and near-inertial oscillations (local inertial period is 19.6 hours) are often observed [*Kim et al.*, 2005a, 2005b, 2001; *Lie et al.*, 1992; *Lie*, 1988]. Particularly, three packets of highly nonlinear ISWs are observed at the interval of the near-inertial period, suggesting the near-inertial (rather than semidiurnal) origin of the ISWs [*Kim et al.*, 2001]. As *Keen and Allen* [2000] and *Gill* [1982] proposed that the near-inertial internal waves would be generated after a hurricane passage, passage of typhoon around the Korean peninsula can be an energy source of ISWs.

[4] Thus, this study aims to answer the following questions. Does a typhoon passage over fine scale topographic features generate highly nonlinear ISWs? If yes, what is the generating mechanism? What are their spatial characteristics and relationship to the local features of bottom topography? The SAR image taken approximately 19 hours after typhoon MAEMI's passage as well as the buoy measurements during the typhoon passage is described in next section. In section 3, the sequential processes are inferred and discussed with conceptual schematics. Finally, the results are summarized in section 4.

2. Observations

2.1. The SAR Image

[5] Figure 2a shows an ENVISAT SAR image over the east coast of Korea acquired at 22:10 (13:10 UTC) on September 13, 2003, approximately 19 hours after typhoon MAEMI's passage across the coastal region at 03:00 on the same date. The image clearly shows two packets of rank-ordered ISWs. Since it is generally accepted that the leading internal soliton in a wave packet is the largest and those solitons that follow are successively smaller as intersolition separations are successively closer, these ISWs appear to travel in opposite directions of each other. The onshore-propagating ISWs (left) show three distinct bright/dark bands while the offshore-propagating ISWs (right) have a higher contrast and more crests (Figures 2a and 2b). The length of packet ranges from 3–7 km in the direction of wave propagation, and the wavelength of individual ISWs is about 0.5 to 1.2 km. Both packets of ISWs propagating onshore and offshore seem to be depression waves because the leading bright bands are immediately followed by dark bands.

[6] It should be noticed that the horizontal structures of wave crests are not parallel to the coastline (Figure 2a). The crests of ISWs in the onshore propagating packet curve in a northeast-southwest direction (NE–SW), whereas those in the offshore propagating packet are aligned to a NNW–SSE direction. This indicates northwestward and east-northeastward propagations of the two packets respectively since the ISWs propagate perpendicular to the wave crest. Generation of those ISWs can be traced back to the past, speculating the

[1]Seoul National University, Seoul, South Korea.
[2]Now at Agency for Defense Development, Chinhae, South Korea.
[3]Department of Naval Architecture and Marine Engineering, University of Michigan, Ann Arbor, Michigan, USA.
[4]Agency for Defense Development, Chinhae, South Korea.

0094-8276/07/2006GL028187

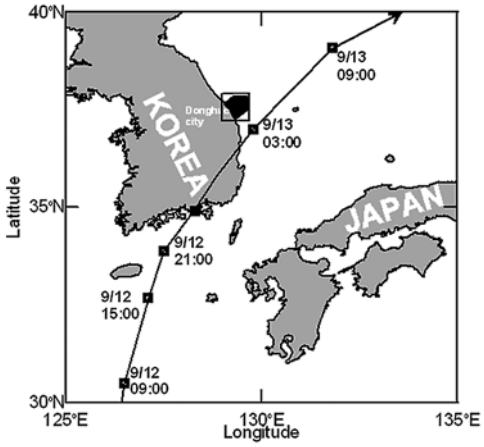

Figure 1. Location around the study area superimposed with track of typhoon MAEMI during September 12–13, 2003. Here, the coastal region off Donghae city, shown by the box, corresponds to the domain of Figure 2.

source region between the two packets. One possible source region is the 'S' area, a region of sharply varying topographic feature (eastward bottom slope locally reaches 0.15) approximately 28 km off the coast with meridional scale of about 10 km (Figures 2c and 2d). The spatial structure of the highly nonlinear ISWs could be like the pattern observed from the SAR image in Figure 2a if they are generated in the 'S' area prior to the time that the SAR image is taken. This hypothesis is investigated with an analysis of in-situ data acquired in the region after the typhoon passage, providing insight on the sequential processes associated with the ISWs evolution.

2.2. Buoy Measurements

[7] The East Sea Real-time Ocean Buoy (ESROB), deployed approximately 8 km off the coast in a depth of 130 m (Figures 2a, 2b, and 2d), recorded a maximum wind gust of 25 m/s and a minimum atmospheric pressure of 980 hPa when the eye of typhoon MAEMI passed close to the buoy (Figure 1) at 03:00 September 13, 2003 [*Nam et al.*, 2004]. After the strong northerly wind event at 03:00 associated with the typhoon, the sequential changes of velocity and temperature were observed by the 300 kHz acoustic Doppler current profiler (ADCP) and five Conductivity-Temperature-Depths (CTDs) sensors attached to the ESROB [*Nam et al.*, 2005]. Here, the buoy measurements for the period from the wind event (03:00) to the time of the SAR image (22:10) are described. The period is divided into five stages (Phase-I: 03:00–08:30, Phase-II: 08:30–11:30, Phase-III: 11:30–13:30, Phase-IV: 13:30–16:10, and Phase-V: 16:10–22:10) as indicated in Figure 3.

[8] During Phase-I, the southward currents slowly increased up to 100 cm/s at 5 m and those at 20 m reached to 50 cm/s without such slow current change at 40, 60, and 100 m (Figure 3a). Strong westward and northward currents (~100 cm/s) were temporally observed at 100 m combined with temporal weakness of southward currents at 5 and 20 m in Phase-II. During Phase-III, the southward currents at 5 m decreased while those at 20 m increased and

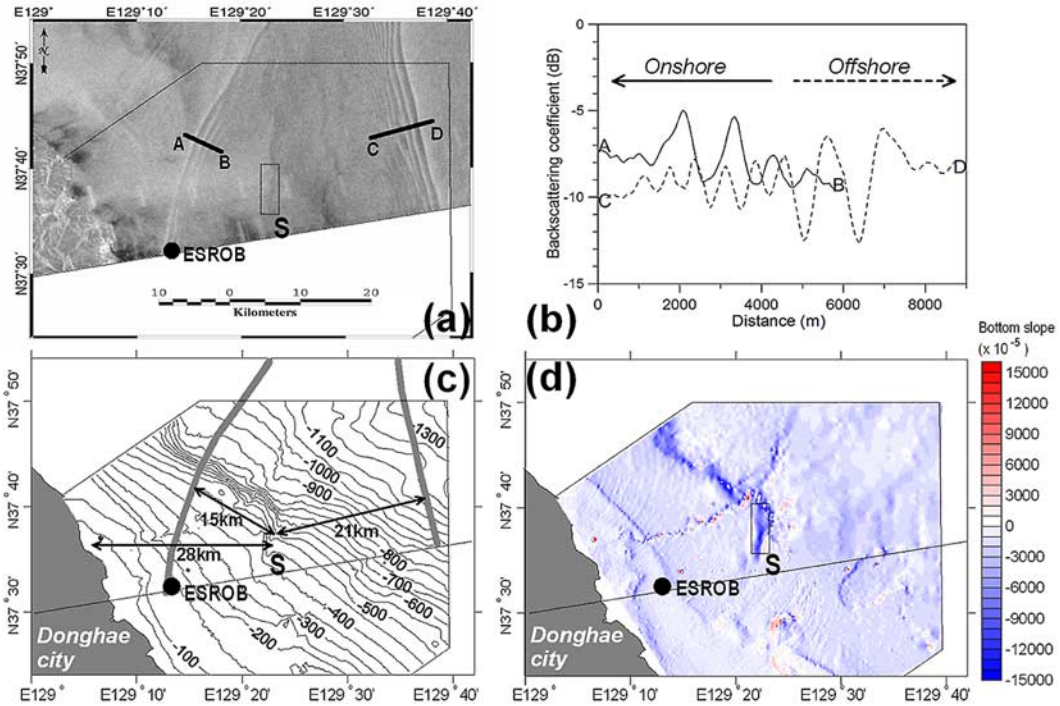

Figure 2. (a) ENVISAT SAR image taken on 22:10 (13:10 UTC) September 13, 2003, (b) backscattering coefficients across the A-B and C-D sections, (c) high resolution (less than 50 m in space) bottom topography, and (d) eastward bottom slope in the coastal region off Donghae city, where the domain of Figures 2a, 2c, and 2d is noted in Figure 1. Surface signatures of highly nonlinear ISWs packets are marked with thick gray curves in Figure 2c. The region of sharply varying topography 28 km off the coast is noted with the symbol 'S' in Figures 2a, 2c, and 2d. Here, the ESROB denotes the East Sea Real-time Ocean Buoy.

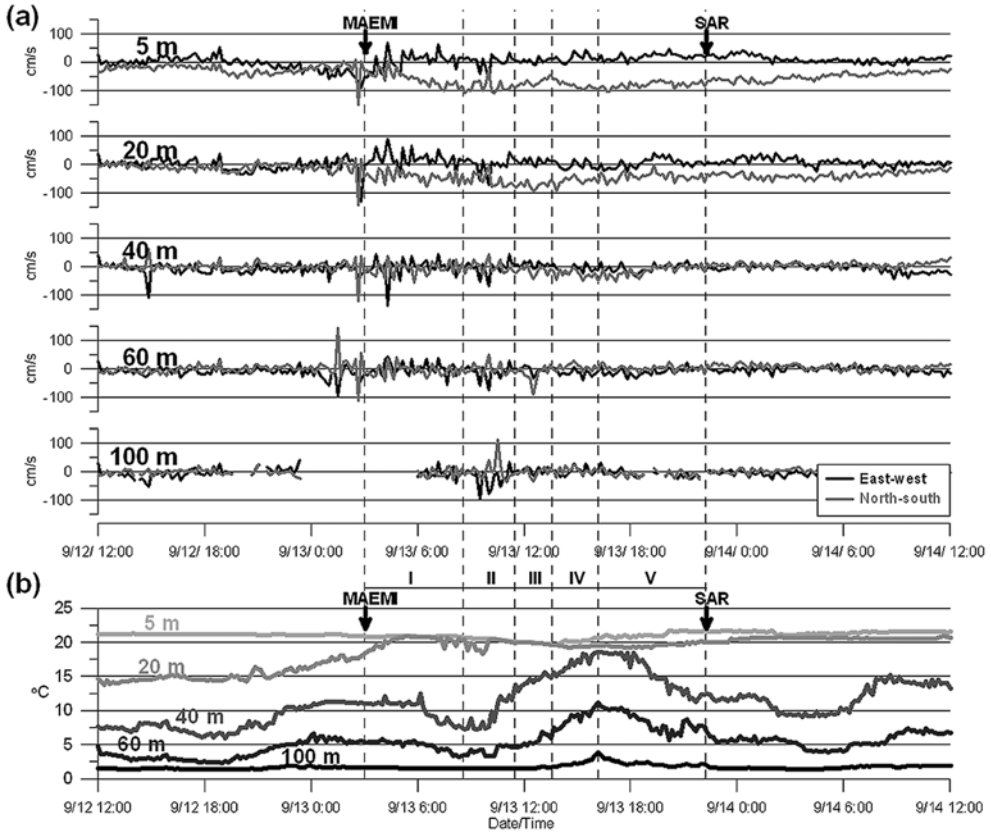

Figure 3. Time series of (a) east-west (black) and north-south (gray) currents and (b) water temperature for 48 hours from 12:00 12 September to 12:00 14 September, 2003, that are measured at 5, 20, 40, 60, and 100 m on the ESROB. The times when the eye of typhoon MAEMI was located at the closest point from the ESROB (03:00 13 September) and when the SAR image was taken (22:10 13 September) are noted in Figures 3a and 3b with arrows labeled by 'MAEMI' and 'SAR', respectively. Here, the vertical dashed lines represent times of 03:00, 08:30, 11:30, 13:30, 16:10, and 22:10 which divide the period of about 19 hours from the MAEMI's passage to the SAR image into five stages (Phase-I, II, III, IV, and V).

reached a maximum of about 100 cm/s around 13:00, approximately 10 hours after the typhoon passage. Then, during Phase-IV, the southward currents at 5 m increased again up to 100 cm/s, whereas those at 20 m slowly decreased. The strong southward currents of 80–100 cm/s at 5 m and 30–40 cm/s at 20 m were maintained for Phase-V.

[9] The surface mixed layer thickness (discerned from the water below by the high temperature and low salinity with the sharp vertical gradients) accompanied by the strong southward current, changed from 20 to 40 m in 10 hours from 03:00 to 13:00 [*Nam et al.*, 2004]. During Phase-I, the temperature measured at 20 m slowly increased from 18°C to 21°C and became nearly the same as the temperature at 5 m (Figure 3b). Slow decreases of temperature at 40 m and 60 m were observed during Phase-I along with a nearly constant temperature (~1.5°C) at 100 m. The temperatures at 40 m and 60 m reached local minima around 10:00 in Phase-II. Then, by Phase-IV, the temperatures at 40 m and 60 m monotonically increased and they reached maxima at 16:10 when the maximum temperature of 3.9°C was also recoded at 100 m. During Phase-V, the temperatures at 40 m and 60 m decreased monotonically with abrupt changes around 21:00 at 60 m. They reached local minima again around 04:00 September 14. The intervals between the two temperature minima (at 10:00 September 13 and 04:00 September 14) correspond to a near-inertial period of 18 hours rather than the semidiurnal period.

[10] Temporal structures of current and temperature observed from Phase-I to Phase-V are summarized as (1) strong southward currents at the upper levels, (2) temperature oscillations near the thermocline, and (3) abrupt temporal changes of the current and temperature. The observations seem to be associated with sequential processes of coastal ocean response to the typhoon passage across the region, specifically the development of strong southward coastal jet at the upper levels (Phase-I to Phase-III), generation of near-inertial waves at the coastal boundary (Phase-II and -III), seaward propagation of near-inertial waves (Phase-IV), generation of ISWs in the 'S' area (16:10), and both onshore and offshore propagations of ISWs (Phase-V). These processes are detailed in the next section.

3. Scenario on Sequential Processes

[11] A simple two layer model for the response to an impulsive alongshore wind over an uniformly sloping bottom provides reasonable estimates of alongshore and cross-shore currents at both layers and interface between the

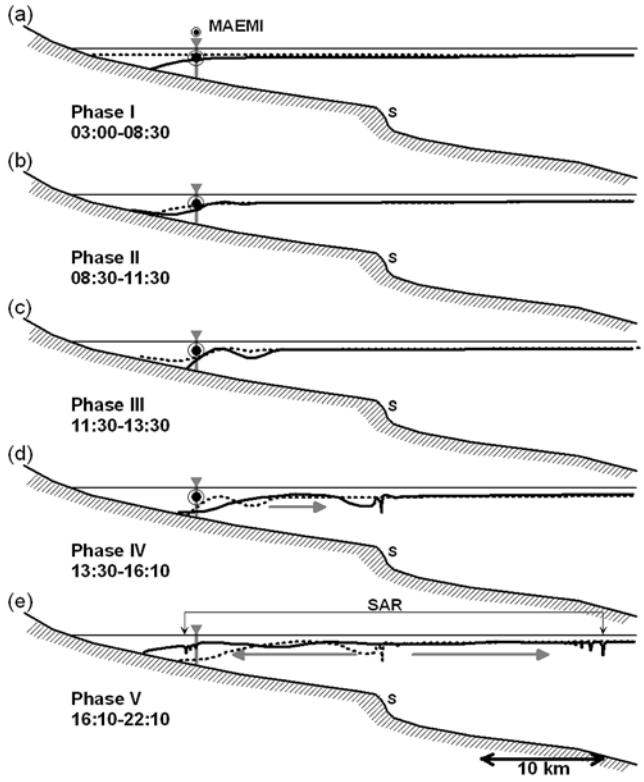

Figure 4. Conceptual schematics of sequential processes with corresponding times on September 13. The stages of (a) developing coastal jet (Phase-I: 03:00–08:30), (b) wind relaxation (Phase-II: 08:30–13:30), (c) developing near-inertial waves (Phase-III: 11:30–13:30), (d) offshore propagation of near-inertial waves (Phase-IV: 13:30–16:10), and (e) propagation of two packets of depression ISWs (Phase-V: 16:10–22:10) are displayed. The interfaces are changed from dashed curves to solid curves. Strong northerly wind event when the eye of typhoon is located nearby and the surface detection of the ISWs are noted in Figures 4a and 4e, respectively, with 'MAEMI' and 'SAR.' Here, the gray vertical sticks denote the position of the ESROB and approximate distance of 10 km is shown in right bottom corner.

layers during 10 hours (03:00–13:00, from Phase-I to Phase-III) after typhoon passage across the region [*Nam et al.*, 2004]. The response to the typhoon MAEMI is similar to the coastal downwelling in the sense that the onshore Ekman drift at the upper layer triggers enhanced vertical shear of alongshore current with the southward coastal jet at the upper layer, sea level rise at coast and interface drop on the sloping bottom (Figure 4a). Relative vorticity (horizontal shear of alongshore currents) offshore of the (downwelling) coastal jet is positive (cyclonic).

[12] After the alongshore wind forcing subsided, the upper ocean starts to oscillate in Phase-II and Phase-III, that is so called inertial oscillations (Figures 4b and 4c). No normal flow condition at the coast requires vertical motion so that the surface inertial oscillations can generate interface oscillations, or (interfacial) near-inertial internal waves. The near-inertial waves freely propagate offshore during Phase-IV (Figure 4d). In particular, the coastal jet of downwelling type acts as a background condition that permit offshore propagation (expelling from the region) of near-inertial waves due to the positive value of relative vorticity [*Davies and Xing*, 2002; *Federiuk and Allen*, 1996]. The speed of the (first baroclinic) near-inertial waves is 2.4 m/s, e.g., $\sqrt{g'h2}$ for the lower layer thickness ($h2$) of 90 m and a reduced gravity ($g' = g(\rho 2 - \rho 1)/\rho 2$) of 6.5×10^{-2} m/s^2, based on the ESROB measurements, which corresponds to 3.2 hours for propagating the distance of 28 km (distance to the 'S' area from the coast). This indicates that the near-inertial waves can arrive in the 'S' area around the time of 16:10 September 13.

[13] When the near-inertial waves encounter the sharply varying topographic feature 28 km off the coast ('S' area), the ISWs of depression can be generated through the interaction between the near-inertial waves and the bottom topography. This topographic feature is well distinguished in the map of bottom slope (Figure 2d). Horizontal speed of instantaneous current of ~1 m/s near the bottom corresponds to the vertical speed of 0.15 m/s (vertical displace-

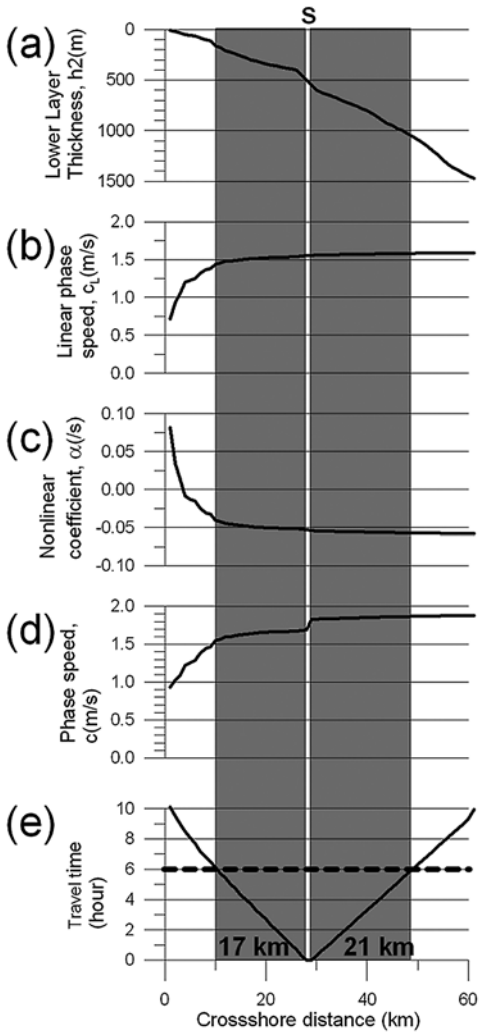

Figure 5. Structure of (a) lower layer thickness (m), (b) linear phase speed (m/s), (c) nonlinear coefficient (/s), (d) phase speed (m/s), and (e) elapsed time for which the ISWs propagate from the 'S' area. Here, the shaded area represents the periods of 6 hours from the time of ISWs generation (16:10) to the time of SAR image taken (22:10).

ments of approximately 10 m in a minute) for the bottom slope of 0.15, which can be a sufficient condition for generating ISWs with the amplitude of a few to few tens of meters as observed in the region [*Kim et al.*, 2001].

[14] Then, for the 6 hours from 16:10 to 22:10 (Phase-V), the two packets of ISWs may propagate approximately 15 km onshore and 21 km offshore (Figures 2b and 4e). The distances that the two packets propagate in both directions during the 6 hours are estimated to 17 km and 21 km respectively with the spatially varying group speeds, i.e., $c_g\ (x) = c(x)/2$ where the phase speed $c(x) = c_L(x) + \alpha(x)\eta_0/3$ (Figure 5d) is calculated based on the two-layered Korteweg-deVries (KdV) equation. The linear phase speed, c_L (Figure 5b), and the nonlinear coefficient, α (Figure 5c), are calculated as below.

$$c_L(x) = \sqrt{\frac{\rho 2 - \rho 1}{\rho 2} g \ \frac{h1 \cdot h2(x)}{h1 + h2(x)}}, \quad \alpha(x) = \frac{3}{2}\frac{h1 - h2(x)}{h1 \cdot h2(x)} c_L(x)$$

Here, the densities at the upper and lower layers ($\rho 1$ and $\rho 2$), and thickness of the upper layer ($h1$) are fixed to 1020.48 kg/m^3, 1027.26 kg/m^3, and 40 m, respectively [*Nam et al.*, 2004], and only the thickness of lower layer ($h2$) varies. The amplitudes (η_0) of onshore and offshore propagating ISWs are set to 8 and 15 m, respectively.

4. Summary

[15] Both onshore and offshore propagating packets of highly nonlinear internal solitary waves (ISWs) are detected in the synthetic aperture radar (SAR) image taken approximately 19 hours after typhoon MAEMI's passage across the east coast of Korea. The East Sea Real-time Ocean Buoy (ESROB) recorded strong southward currents at the upper levels, temperature oscillations near the thermocline, and abrupt temperature changes. Based on the time series measurements, a concept of sequential processes associated with the ISWs captured in the SAR image are suggested, specifically development of a coastal jet, generation of near-inertial waves, seaward propagation of near-inertial waves, generation of ISWs in the 'S' area 28 km off the coast, and propagation of ISWs in both onshore and offshore directions. The distances that the ISWs propagate for 6 hours, estimated based on the two-layered Korteweg-deVries (KdV) equation (upper layer thickness and densities at both layers are fixed), are consistent with the distance of detected ISWs from the 'S' area.

[16] **Acknowledgments.** Authors are grateful to K. Kim of Seoul National University (SNU) for his careful help in revising original manuscript. The SAR image we use in this study is generously provided by W. M. Moon of SNU. The ESROB is developed and maintained together with OTRONIX Group by RIO, SNU, in support of the Korean Ministry of Science and Technology through the NRL (2000-N-NL-01-C-012), the Agency for Defense Development (609-83-01532, UD000008BD, UD970022AD). Partial supports are also provided by the Korean Ministry of Environments (121-041-033). The first author is supported by the Korean Ministry of Education through the BK21-SEES program and also by the Korean Research Foundation through the Free-Doctoral Scholars program. The second author is supported by the Korean Research Foundation Grant funded by the Korean Government (KRF-2005-214-C00239).

References

Alpers, W. (1985), Theory of radar imaging of internal waves, *Nature*, *314*, 245–247.

Brandt, P., A. Rubino, W. Alpers, and J. O. Backhaus (1997), Internal waves in the Strait of Messina studied by a numerical model and synthetic aperture radar images from the ERS-1/2 satellites, *J. Phys. Oceanogr.*, *27*, 648–663.

Davies, A. M., and J. Xing (2002), Influence of coastal fronts on near-inertial internal waves, *Geophys. Res. Lett.*, *29*(23), 2114, doi:10.1029/2002GL015904.

Federiuk, J., and J. S. Allen (1996), Model studies of near-inertial waves in flow over the Oregon continental shelf, *J. Phys. Oceanogr.*, *26*, 2053–2075.

Gill, A. E. (1982), *Atmosphere-Ocean Dynamics*, Elsevier, New York.

Keen, T. R., and S. E. Allen (2000), The generation of internal waves on the continental shelf by Hurricane Andrew, *J. Geophys. Res.*, *105*, 26,203–26,224.

Kim, D., S. Nam, H. R. Kim, W. M. Moon, and K. Kim (2005a), Can near-inertial internal waves in the East Sea be observed by synthetic aperture radar?, *Geophys. Res. Lett.*, *32*, L02606, doi:10.1029/2004GL021532.

Kim, H.-J., Y.-G. Park, and K. Kim (2005b), Generation mechanism of near-inertial internal waves observed off the east coast of Korea, *Cont. Shelf Res.*, *25*, 1712–1719.

Kim, H.R., S. Ahn, and K. Kim (2001), Observations of highly nonlinear internal solitons generated by near-inertial internal waves off the east coast of Korea, *Geophys. Res. Lett.*, *28*(16), 3191–3194.

Klymak, J. M., R. Pinkel, C.-T. Liu, A. K. Liu, and L. David (2006), Prototypical solitons in the South China Sea, *Geophys. Res. Lett.*, *33*, L11607, doi:10.1029/2006GL025932.

Lie, H. (1988), Near-inertial current oscillations off the mid-east coast of Korea, *Prog. Oceanogr.*, *21*, 241–253.

Lie, H.-J., C.-W. Shin, and Y. H. Seung (1992), Internal tidal oscillations of temperature off Jukbyun on the east coast of Korea, *J. Oceanol. Soc. Korea*, *27*, 228–236.

Moum, J. N., D. M. Farmer, W. D. Smyth, L. Armi, and S. Vagle (2003), Structure and generation of turbulence at interfaces strained by internal solitary waves propagating shoreward over the continental shelf, *J. Phys. Oceanogr.*, *33*, 2093–2112.

Nam, S. H., J.-Y. Yun, and K. Kim (2004), Observations on the coastal ocean response to typhoon MAEMI at the East Sea Real-time Ocean Buoy (in Korean with English abstract), *J. Korean Soc. Oceangr.*, *9*(3), 111–118.

Nam, S. H., G. Kim, K. R. Kim, K. Kim, L. O. Cheng, K. W. Kim, H. Ossi, and Y. G. Kim (2005), Application of real-time monitoring buoy systems for physical and biogeochemical parameters in the coastal ocean around the Korean peninsula, *Mar. Technol. Soc. J.*, *39*, 70–80.

Nash, J. D., and J. N. Moum (2005), River plumes as a source of large-amplitude internal waves in the coastal ocean, *Nature*, *437*, 400–403, doi:10.1038/nature03936.

Zhao, Z., V. Klemas, Q. Zheng, and X.-H. Yan (2004), Remote sensing evidence for baroclinic tide origin of internal solitary waves in the northeastern South China Sea, *Geophys. Res. Lett.*, *31*, L06302, doi:10.1029/2003GL019077.

D. Kim, Department of Naval Architecture and Marine Engineering, University of Michigan, Ann Arbor, MI 48109, USA. (djkkim@umich.edu)

H. R. Kim, Y.-G. Kim, and S. Nam, Agency for Defense Development, Chinhae 645-016, South Korea. (hyoungrok@add.re.kr; youngkim@add.re.kr; namsh6513@add.re.kr)